In Situ Derived Bi Nanoparticles Confined in Carbon Rods as an Efficient Electrocatalyst for Ambient N_2 Reduction to NH_3

Fengyi Wang, Longcheng Zhang, Ting Wang, Fang Zhang, Qian Liu, Haitao Zhao, Baozhan Zheng,* Juan Du,* and Xuping Sun*

Cite This: https://doi.org/10.1021/acs.inorgchem.1c01130

Read Online

| ACCESS | | Metrics & More | | Article Recommendations | | Supporting Information |

ABSTRACT: Electrocatalytic N_2 reduction is deemed as a prospective strategy toward low-carbon and environmentally friendly NH_3 production under mild conditions, but its further application is still plagued by low NH_3 yield and poor faradaic efficiency (FE). Thus, electrocatalysts endowing with high activity and satisfying selectivity are highly needed. Herein, Bi nanoparticles in situ confined in carbon rods (Bi NPs@CRs) are reported, which are fabricated via thermal annealing of a Bi-MOF precursor as a high-efficiency electrocatalyst for artificial NH_3 synthesis with favorable selectivity. Such an electrocatalyst conducted in 0.1 M HCl achieves a high FE of 11.50% and a large NH_3 yield of 20.80 μg h^{-1} mg$^{-1}_{cat.}$ at -0.55 and -0.60 V versus reversible hydrogen electrode, respectively, which also possesses high electrochemical durability.
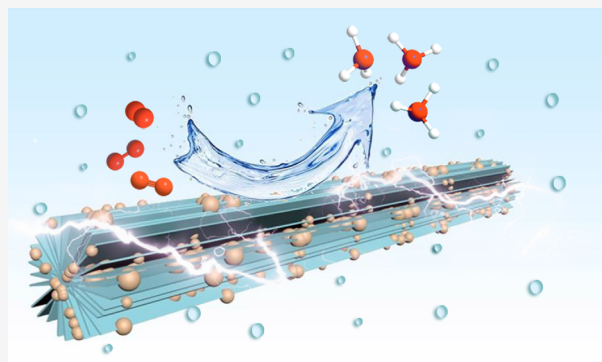
INTRODUCTION

As one of the most essential raw materials, NH_3 has been extensively employed to make fertilizer and pharmaceutical production.[1−3] Moreover, it also can be used as an ideal green carbon-free energy carrier and potential transportation fuel.[4] Nevertheless, industrial scalable production of NH_3 is commonly through the Haber−Bosch process with H_2 and N_2 as synthesis gas, which is operated at severe synthetic conditions, accompanied by massive CO_2 emission.[5,6] Therefore, an energy-saving and environmentally friendly approach for NH_3 synthesis is in urgent demand.

Electrochemical N_2 reduction is an alternative route for realizing sustainable ambient NH_3 synthesis,[7−10] yet the high chemical inertness of a N≡N triple bond is hard to break in a chemical reaction.[11−13] It is reported that noble metals can efficiently activate N_2, but their practical scalable applications in N_2 reduction reaction (NRR) are still restricted by high cost and scarcity.[14−18] Research focus of NRR has thus transferred into noble-metal-free alternatives.[19−32]

Bi-based catalysts are appealing for an intriguing candidate for an efficient NRR electrocatalyst due to their intrinsic catalytic activity, earth-abundance, low cost, and eco-friendliness.[33−36] Meantime, Bi as a main group metal with tunable p-electron density can selectively promote the reductive absorption of N_2 to form N_2H^* but has no effect on the binding energy of the later intermediates, and also confines the surface electron accessibility, thus suppressing the HER process.[37,38] Currently, encouraging advances have been gained for the NRR on Bi-based electrocatalysts such as Bi

nanosheet,[36] mosaic Bi nanosheet,[37] and Bi nanodendrite.[39] Apart from precisely tuning the morphology, researchers also focus on decreasing the size or increasing the dispersity of Bi nanoparticles (Bi NPs).[40,41] Previous research reported that reducing the size of catalysts or increasing the dispersity can efficiently increase the surface area of catalysts, thus exposing more active sites, leading to enhancement of electrochemical performances.[41,42] However, major problems of self-aggregation caused by downsizing particle size and intrinsic low conductivity impose the electrochemical performance of Bi NPs.[21,35] Aimed at overcoming these problems hereinbefore, using a carbon matrix as a conductive skeleton can improve its electrical conductivity and support the active particles to restrain their aggregation. Moreover, in situ forming Bi NPs confined in a carbon scaffold would suppress the further growth of Bi NPs to reduce the size to some extent. So, it is promising to design Bi NPs confined in carbon rods derived from a MOF as electrocatalyst for the NRR, which, however, has not been reported before.

Herein, we report that Bi NPs uniformly entrapped in MOF derived carbon rods (Bi NPs@CRs) can perform favorable NRR performance under ambient conditions. When tested in

0.1 M HCl, a high FE (11.50%) and a large NH_3 yield (20.80 $\mu g\ h^{-1}\ mg^{-1}_{cat.}$) for Bi NPs@CRs have been achieved at −0.55 and −0.60 V versus reversible hydrogen electrode (RHE), respectively.

■ RESULTS AND DISCUSSION

The Bi NPs@CRs were synthesized via thermal solvent refluxing, followed by a facile annealing method in an Ar atmosphere as illustrated in Figure 1a. The X-ray diffraction
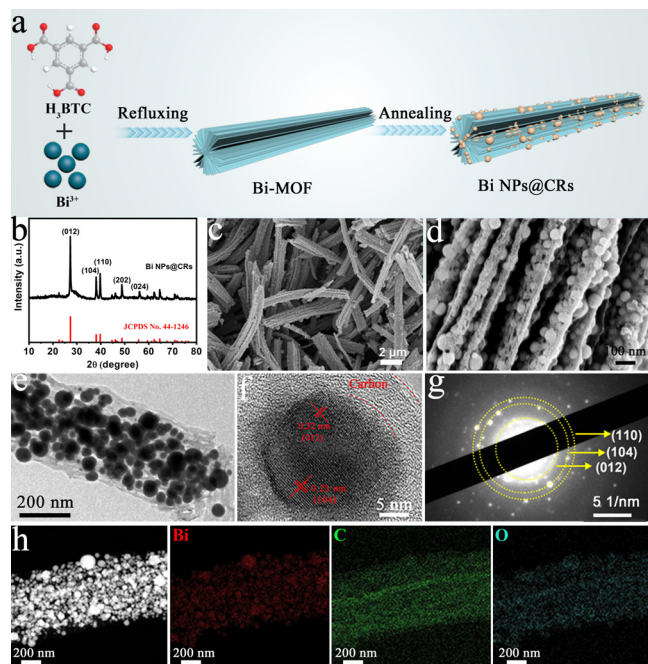

Figure 1. (a) Brief illustration of the synthesis process of Bi NPs@CRs. (b) XRD pattern, (c, d) SEM images, (e, f) TEM images, and (g) selected area diffraction of Bi NPs@CRs. (h) STEM image and the elemental mapping images of Bi, C, O, for Bi NPs@CRs.

(XRD) pattern of the as-synthesized Bi-MOF using an organic ligand (H_3BTC) as linker shows typical diffraction peaks, which are consistent with reported theoretical data (Figure S1).[43,44] In terms of Bi NPs@CRs, the noticeable diffraction peaks of Figure 1b at 27.2°, 37.9°, 39.6°, 48.7°, and 55.6° are indexed to the (012), (104), (110), (202), and (024) planes of the Bi phase (JCPDS No. 44-1246), respectively. The wide peaks ranging from 20° to 30° may be ascribed to the carbon shell forming in the annealing process.[45] Furthermore, the morphology and structure of the Bi-MOF and Bi NPs@CRs were investigated through scanning electron microscopy (SEM) and transmission electron microscopy (TEM). Figure S2 shows that the precursor of Bi-MOF presents a rod structure with a smooth surface. After annealing, the Bi NPs@CRs still hold the rod morphology as presented in Figure 1c, but the Bi NPs are evenly confined into the carbon framework observed from the high-magnification SEM image (Figure 1d). The TEM (Figure 1e) with low magnification and the high-resolution TEM (HRTEM) presented in Figure 1f demonstrate that the Bi NPs are entrapped by a carbon layer with a thickness of less than 10 nm. Moreover, the selected-area electron diffraction (SAED) pattern shown in Figure 1g reveals that the interlayer distance of lattice fringes is 0.32 and 0.23 nm, which are indexed to the (012) and (104) planes of metal Bi. Besides, the STEM coupled with related energy dispersive

X-ray (EDX) elemental mapping images further indicates that Bi NPs are uniformly distributed in the carbon framework (Figure 1h).

The X-ray photoelectron spectroscopy (XPS) survey spectrum of Bi NPs@CRs shows three elements of Bi, C, and O (Figure 2a). Figure 2b reveals the XPS spectrum in the
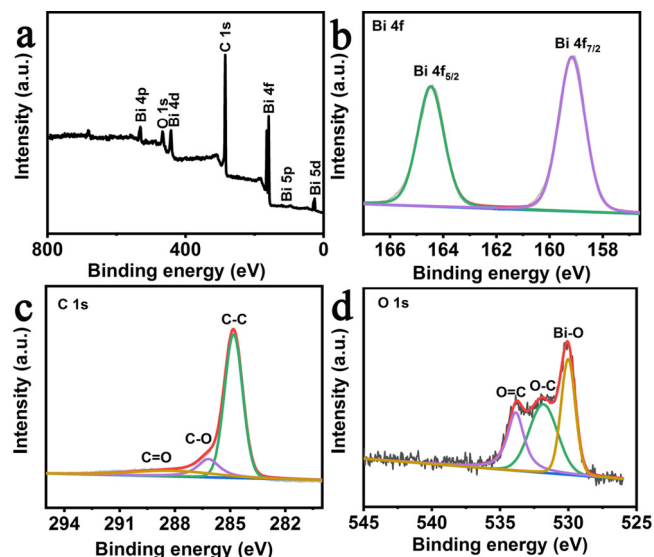

Figure 2. (a) XPS survey spectrum of Bi NPs@CRs in Bi 4f (b), C 1s (c), and O 1s (d) regions.

Bi 4f region, revealing two distinct peaks with binding energies (BEs) of Bi $4f_{7/2}$ and $4f_{5/2}$ located at 159.2 and 164.5 eV, respectively. These results are corresponding to the BEs for Bi metal, which is in accordance with XRD and TEM data.[46,47] Figure 2c shows the region of C 1s; the peak values of BEs situated in 284.8, 286.2, and 288.1 eV belong to the single bonds of C−C and C−O and the double bond of C═O in the carbon framework, respectively.[48] The results of Figure 2d show that the O 1s region spectrum has three obvious peaks at 530.0, 531.8, and 533.8 eV, which are ascribed to the Bi−O, O═C, and O−C bonds, respectively.[49] The Bi−O bond may be attributed to superficial oxidation of as-prepared material.

The electrocatalytic NRR characteristics of Bi NPs@CRs in 0.1 M HCl electrolyte were implemented in an electrolytic cell disconnected through a Nafion membrane (117). Carbon paper was used as conductive matrix to deposit the Bi NPs@CRs (loading amount of Bi NPs@CRs/CP: 0.1 mg cm⁻²), which serves as working electrode. Saturated KCl solution filling in Ag/AgCl behaves as reference, yet a graphite rod acted as counter electrode. Additionally, the RHE scale is commonly used to calibrate all applied potentials during the electrocatalytic process. Linear sweep voltammetry of Bi NPs@CRs/CP performed in 0.1 M HCl electrolyte with high purity N_2 and Ar as supplied gas until saturated is illustrated in Figure S3; the red curve gained by N_2-bubbling has a slightly higher catalytic current, confirming Bi NPs@CRs/CP has catalytic activity for N_2 conversion to NH_3 under moderate conditions. The indophenol blue method[50] is utilized for the determination of generated NH_3, while the approach of Watt and Chrisp is used to examine the potential byproduct of N_2H_4.[51] The corresponding calibration curves are provided in Figures S4 and S5. The chronoamperometry curves of Bi NPs@CRs/CP displayed in Figure 3a are operated at a set of potentials
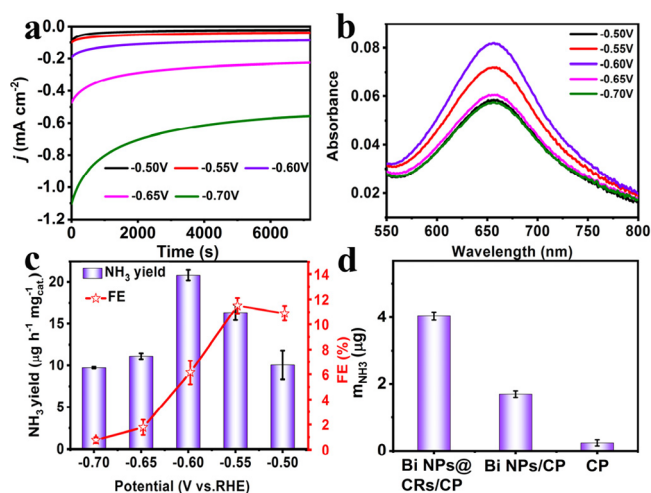
Figure 3. (a) Chronoamperometry data of Bi NPs@CRs/CP at a set of potentials. (b) UV−vis spectra of the electrolytes after NRR electrolysis kept for 2 h. (c) Gained NH_3 yields and FEs of Bi NPs@CRs/CP at certain potentials. (d) Gained corresponding NH_3 amount with Bi NPs@CRs/CP, Bi NPs/CP, and CP at −0.60 V vs RHE.

from −0.50 to −0.7 V in acidic electrolyte (HCl, pH = 1), inletting N_2 until saturated for 2 h. After that, the color reagent of as-prepared indophenol was utilized to dye with the electrolytes after electrolysis in dark circumstance, and UV−vis absorption spectra in different potentials can be observed from Figure 3b. According to relevant calibration curves (Figure S4), the calculated average values of NH_3 yields and FEs for Bi NPs@CRs/CP are plotted in Figure 3c.

Clearly, a high NH_3 yield of 20.80 $\mu g\ h^{-1}\ mg^{-1}_{cat.}$ for Bi NPs@CRs/CP delivers at −0.60 V, yet the high FE of 11.50% is achieved at −0.55 V, both of which are superior to previous reported data based on aqueous NRR catalysts (Table S1). As presented, the NH_3 yields and corresponding FEs reduce obviously when the potential value exceeds −0.60 V; these results may be ascribed to the competitive process toward HER.[52] Furthermore, the possible byproduct of N_2H_4 has not been detected as illustrated in Figure S6, manifesting that Bi NPs@CRs/CP has excellent selectivity for NH_3.

The excellent NRR performance of Bi NPs@CRs needed to be further confirmed through a series of control experiments. Bi NPs (Figures S7 and S8) were synthesized through a hydrothermal approach. As a comparison, the NRR properties of blank CP and Bi NPs/CP are then contrasted with those of Bi NPs@CRs/CP at −0.60 V. Obviously, these results illustrated in Figure 3d demonstrate that blank CP and Bi NPs/CP yield 0.23 and 1.69 μg at −0.60 V through electrolysis kept for 2 h, respectively. Such values are inferior to that of Bi NPs@CRs/CP (4.03 μg) under the same conditions. The prominent enhancement of NRR performance for Bi NPs@CRs/CP may be ascribed to the Bi NPs with an average size counted by 28.7 nm uniformly distributed on carbon rods; this feature facilitates more active sites exposure, thus benefiting the NRR progress as displayed in Figures S9 and S10.[53] In order to verify the reliability of spectrophotometry, ion chromatography is offered to analyze the NH_3 yields and related FEs at different applied potentials. The data of ion chromatography illustrated in Figure S11 are comparable with the counterpart obtained through the method of indophenol blue.

The N source is required to further validate that the generated NH_3 indeed originated from the electrocatalytic N_2 reduction process. We first confirmed whether nitrate and nitrite existed in the supernatant of as-annealed Bi NPs@CRs; the results of Figures S12 and S13 indicated that the NO_3^- and NO_2^- in the supernatant of washed material were indeed not present after the annealing procedure, which eliminates nitrate and nitrite contribution to NRR. After that, several control experiments are conducted at −0.6 V, such as under open circuit and Ar-saturated electrolyte. Obviously, no distinct NH_3 is determined under open circuit and Ar conditions as shown in Figure 4a. Moreover, the electrochemical tests are
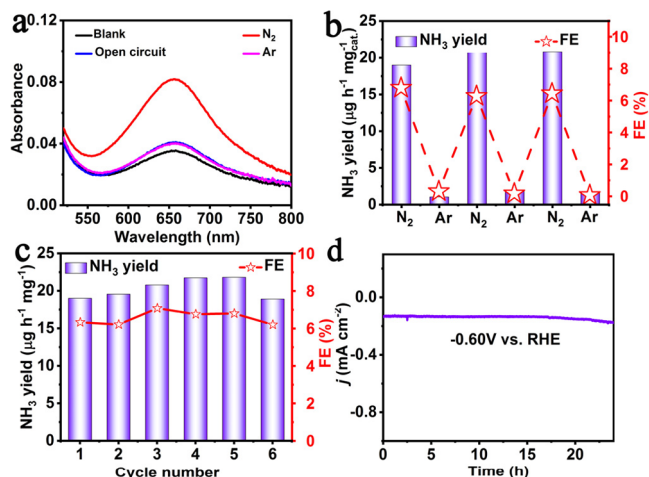
Figure 4. (a) UV−vis absorption spectra of the electrolytes colored with indophenol reagent utilizing Bi NPs@CRs/CP at different performing conditions. (b) Gained NH_3 yields and FEs of Bi NPs@CRs/CP under N_2- and Ar-dominated electrolytes for 2 h. (c) Six circulating measurements of Bi NPs@CRs/CP at −0.60 V. (d) The chronoamperometry curve for Bi NPs@CRs/CP at −0.60 V for 24 h.

conducted in N_2 and Ar as supplying gas after electrolysis for 2 h. As expected, the NH_3 can only be detected in electrolyte with N_2 as feeding gas (Figure 4b). Furthermore, ^{15}N and ^{14}N isotopic labeling experiments were also conducted to confirm the source of NH_3. The ^1H nuclear magnetic resonance (^1H NMR) spectroscopy of Figure S14 manifests that $^{15}NH_4^+$ with doublet coupling (J = 72 Hz) or $^{14}NH_4^+$ with triplet coupling (J = 52 Hz) only can be observed under $^{15}N_2$ or $^{14}N_2$ as the feeding gas. The above experimental results forcefully manifest that the NH_3 detected by UV−vis absorption spectra is indeed derived from the NRR of Bi NPs@CRs in N_2-saturated solution. Taking into consideration the small amounts of ammonia in air or gas supplied (N_2/Ar), high-purity (99.999%) N_2 or Ar gas flowed into the H-type cell with 0.1 M HCl as electrolyte without applied potential. Corresponding UV−vis curves demonstrate that no obvious NH_3 was detected in air and N_2/Ar (Figure S15).

Stability as another key advantageous feature also can be used for assessing the catalyst performance. Thus, six recycling experiments as presented in Figure 4c were conducted in 0.1 M HCl electrolyte. Small fluctuation can be observed on NH_3 yields and FEs. Furthermore, the corresponding current density and UV−vis absorption spectra also display slight variation (Figure S16a,b). Besides, the chronoamperometry curves (Figure 4d) display mild variation even after 24 h of electrolysis. Also, the Bi NPs@CRs/CP electrolyzed for 24 h

was further performed in fresh HCl solution (pH = 1). UV–vis absorption spectra (Figure S17) illustrate that the absorbance spectra of initial and after electrolysis for 24 h have no apparent decrease. These experimental results reveal that Bi NPs@CRs/CP has excellent electrochemical durability for NRR at ambient conditions. Furthermore, the XRD pattern and SEM image of Bi NPs@CRs/CP after long-term NRR tests also were performed. Figures S18 and S19 demonstrated that Bi NPs@CRs/CP possesses high structure stability for the N_2 reduction.

■ CONCLUSION

To sum up, well-dispersed Bi NPs confined in a carbon framework have been successfully prepared by a Bi-MOF precursor using thermal annealing. This catalyst shows favorable NRR electrochemical performance. In acid solution (0.1 M HCl), the as-fabricated electrocatalyst gained a high NH_3 yield (20.80 $\mu g \ h^{-1} \ mg^{-1}_{cat.}$) at −0.60 V and a high FE (11.50%) at −0.55 V. Our recent findings open up a general route to develop well-dispersed metal nanoparticles confined in conductive carbon nanomaterials derived MOFs for N_2 fixation.

■ ASSOCIATED CONTENT

ⓈⒾ Supporting Information

The Supporting Information is available free of charge at https://pubs.acs.org/doi/10.1021/acs.inorgchem.1c01130.

> Experimental section; XRD patterns; SEM images; UV– vis absorption spectra; Table S1 (PDF)

■ AUTHOR INFORMATION

Corresponding Authors

Baozhan Zheng − *College of Chemistry, Sichuan University, Chengdu 610064, Sichuan, China;* ⓞ orcid.org/0000-0003-4060-5912; Email: zhengbaozhan@scu.edu.cn

Juan Du − *College of Chemistry, Sichuan University, Chengdu 610064, Sichuan, China;* ⓞ orcid.org/0000-0003-3483-8680; Email: dujuanchem@scu.edu.cn

Xuping Sun − *Institute of Fundamental and Frontier Sciences, University of Electronic Science and Technology of China, Chengdu 610054, Sichuan, China;* ⓞ orcid.org/0000-0002-5326-3838; Email: xpsun@uestc.edu.cn

Authors

Fengyi Wang − *College of Chemistry, Sichuan University, Chengdu 610064, Sichuan, China; Institute of Fundamental and Frontier Sciences, University of Electronic Science and Technology of China, Chengdu 610054, Sichuan, China*

Longcheng Zhang − *College of Chemistry, Sichuan University, Chengdu 610064, Sichuan, China; Institute of Fundamental and Frontier Sciences, University of Electronic Science and Technology of China, Chengdu 610054, Sichuan, China*

Ting Wang − *Institute of Fundamental and Frontier Sciences, University of Electronic Science and Technology of China, Chengdu 610054, Sichuan, China*

Fang Zhang − *National Engineering Research Center for Nanotechnology, Shanghai 200241, China*

Qian Liu − *Institute of Fundamental and Frontier Sciences, University of Electronic Science and Technology of China, Chengdu 610054, Sichuan, China;* ⓞ orcid.org/0000-0002-7217-5083

Haitao Zhao − *Materials and Interfaces Center, Shenzhen Institutes of Advanced Technology, Chinese Academy of Sciences, Shenzhen 518055, Guangdong, China*

Complete contact information is available at:
https://pubs.acs.org/10.1021/acs.inorgchem.1c01130

Notes

The authors declare no competing financial interest.

■ ACKNOWLEDGMENTS

■ REFERENCES

(1) Schlögl, R. Catalytic Synthesis of Ammonia-A "Never-Ending Story"? *Angew. Chem., Int. Ed.* **2003**, *42*, 2004−2008.

(2) Gao, S.; Zhu, Y.; Chen, Y.; Tian, M.; Yang, Y.; Jiang, T.; Wang, Z. Self-Power Electroreduction of N_2 into NH_3 by 3D Printed Triboelectric Nanogenerators. *Mater. Today* **2019**, *28*, 17−24.

(3) Rosca, V.; Duca, M.; de Groot, M. T.; Koper, M. T. M. Nitrogen Cycle Electrocatalysis. *Chem. Rev.* **2009**, *109*, 2209−2244.

(4) Klerke, A.; Christensen, C.; Nørskov, J.; Vegge, T. Ammonia for Hydrogen Storage: Challenges and Opportunities. *J. Mater. Chem.* **2008**, *18*, 2304−2310.

(5) Ertl, G. In *Catalytic Ammonia Synthesis*; Jennings, J. R., Ed.; Plenum: New York, 1991.

(6) Dybkjaer, I. In *Ammonia: Catalysis and Manufacture*; Nielsen, A., Ed.; Springer: Heidelberg, 1995; pp 199−308.

(7) Liu, Y.; Li, Q.; Guo, X.; Kong, X.; Ke, J.; Chi, M.; Li, Q.; Geng, Z.; Zeng, J. A Highly Efficient Metal-Free Electrocatalyst of F-Doped Porous Carbon toward N_2 Electroreduction. *Adv. Mater.* **2020**, *32*, 1907690.

(8) Ma, B.; Zhao, H.; Li, T.; Liu, Q.; Luo, Y.; Li, C.; Lu, S.; Asiri, A. M.; Ma, D.; Sun, X. Iron-Group Electrocatalysts for Ambient Nitrogen Reduction Reaction in Aqueous Media. *Nano Res.* **2021**, *14*, 555−569.

(9) Cao, N.; Chen, Z.; Zang, K.; Xu, J.; Zhong, J.; Luo, J.; Xu, X.; Zheng, G. Doping Strain Induced Bi-Ti^{3+} Pairs for Efficient N_2 Activation and Electrocatalytic Fixation. *Nat. Commun.* **2019**, *10*, 2877.

(10) Guo, X.; Du, H.; Qu, F.; Li, J. Recent Progress in Electrocatalytic Nitrogen Reduction. *J. Mater. Chem. A* **2019**, *7*, 3531−3543.

(11) Wu, T.; Zhao, H.; Zhu, X.; Xing, Z.; Liu, Q.; Liu, T.; Gao, S.; Lu, S.; Chen, G.; Asiri, A. M.; Zhang, Y.; Sun, X. Identifying the Origin of Ti^{3+} Activity Toward Enhanced Electrocatalytic N_2 Reduction over TiO_2 Nanoparticles Modulated by Mixed-Valent Copper. *Adv. Mater.* **2020**, *32*, 2000299.

(12) Liu, Y.; Han, M.; Xiong, Q.; Zhang, S.; Zhao, C.; Gong, W.; Wang, G.; Zhang, H.; Zhao, H. Dramatically Enhanced Ambient Ammonia Electrosynthesis Performance by In-Operando Created Li− S Interactions on MoS_2 Electrocatalyst. *Adv. Energy Mater.* **2019**, *9*, 1803935.

(13) Gao, J.; Lv, X.; Wang, F.; Luo, Y.; Lu, S.; Chen, G.; Gao, S.; Zhong, B.; Guo, X.; Sun, X. Enabling Electrochemical Conversion of N_2 to NH_3 under Ambient Conditions by a CoP_3 Nanoneedle Array. *J. Mater. Chem. A* **2020**, *8*, 17956−17959.

(14) Bao, D.; Zhang, Q.; Meng, F. L.; Zhong, H. X.; Shi, M. M.; Zhang, Y.; Yan, J. M.; Jiang, Q.; Zhang, X. B. Electrochemical Reduction of N_2 under Ambient Conditions for Artificial N_2 Fixation and Renewable Energy Storage Using N_2/NH_3 Cycle. *Adv. Mater.* **2017**, *29*, 1604799.

(15) Nazemi, M.; Panikkanvalappil, S. R.; El-Sayed, M. A. Enhancing the Rate of Electrochemical Nitrogen Reduction Reaction for

Ammonia Synthesis under Ambient Conditions Using Hollow Gold Nanocages. *Nano Energy* **2018**, *49*, 316−323.

(16) Zhao, R.; Liu, C.; Zhang, X.; Zhu, X.; Wei, P.; Ji, L.; Guo, Y.; Gao, S.; Luo, Y.; Wang, Z.; Sun, X. A Ultrasmall Ru$_2$P Nanoparticles-Reduced Raphene Oxide Hybrid: An Efficient Electrocatalyst or NH$_3$ Synthesis under Ambient Conditions. *J. Mater. Chem. A* **2020**, *8*, 77−81.

(17) Shi, M.; Bao, D.; Li, S. J.; Wulan, B. R.; Yan, J.; Jiang, Q. Anchoring PdCu Amorphous Nanocluster on Graphene for Electrochemical Reduction of N$_2$ to NH$_3$ under Ambient Conditions in Aqueous Solution. *Adv. Energy Mater.* **2018**, *8*, 1800124.

(18) Deng, G.; Wang, T.; Alshehri, A. A.; Alzahrani, K. A.; Wang, Y.; Ye, H.; Luo, Y.; Sun, X. Improving the Electrocatalytic N$_2$ Reduction Activity of Pd Nanoparticles through Surface Modification. *J. Mater. Chem. A* **2019**, *7*, 21674−21677.

(19) Yang, X.; Nash, J.; Anibal, J.; Dunwell, M.; Kattel, S.; Stavitski, E.; Attenkofer, K.; Chen, J. G.; Yan, Y.; Xu, B. Mechanistic Insights into Electrochemical Nitrogen Reduction Reaction on Vanadium Nitride Nanoparticles. *J. Am. Chem. Soc.* **2018**, *140*, 13387−13391.

(20) Wei, P.; Geng, Q.; Channa, A. I.; Tong, X.; Luo, Y.; Lu, S.; Chen, G.; Gao, S.; Wang, Z.; Sun, X. Electrocatalytic N$_2$ Reduction to NH$_3$ with High Faradaic Efficiency Enabled by Vanadium Phosphide Nanoparticle on V Foil. *Nano Res.* **2020**, *13*, 2967−2972.

(21) Wang, Y.; Shi, M.-m.; Bao, D.; Meng, F.-l.; Zhang, Q.; Zhou, Y.-t.; Liu, K.-h.; Zhang, Y.; Wang, J.-z.; Chen, Z.-w.; Liu, D.-p.; Jiang, Z.; Luo, M.; Gu, L.; Zhang, Q.-h.; Cao, X.-z.; Yao, Y.; Shao, M.-h.; Zhang, Y.; Zhang, X.-B.; Chen, J. G.; Yan, J.-m.; Jiang, Q. Generating Defect-Rich Bismuth for Enhancing the Rate of Nitrogen Electroreduction to Ammonia. *Angew. Chem.* **2019**, *131*, 9564−9569.

(22) Li, C.; Yu, J.; Yang, L.; Zhao, J.; Kong, W.; Wang, T.; Asiri, A. M.; Li, Q.; Sun, X. Spinel LiMn$_2$O$_4$ Nanofiber: An Efficient Electrocatalyst for N$_2$ Reduction to NH$_3$ under Ambient Conditions. *Inorg. Chem.* **2019**, *58*, 9597−9601.

(23) Feng, J.; Zhu, X.; Chen, Q.; Xiong, W.; Chen, X.; Luo, Y.; Alshehri, A. A.; Alzahrani, A. A.; Jiang, Z.; Li, W. Ultrasmall V$_8$C$_7$ Nanoparticles Embedded in Conductive Carbon for Efficient Electrocatalytic N$_2$ Reduction toward Ambient NH$_3$ Production. *J. Mater. Chem. A* **2019**, *7*, 26227−26230.

(24) Cheng, X.; Wang, J.; Xiong, W.; Wang, T.; Wu, T.; Lu, S.; Chen, G.; Gao, S.; Shi, X.; Jiang, Z.; Niu, X.; Sun, X. Greatly Enhanced Electrocatalytic N$_2$ Reduction over V$_2$O$_3$/C by P Doping. *ChemNanoMat* **2020**, *6*, 1315−1319.

(25) He, C.; Wu, Z. Y.; Zhao, L.; Ming, M.; Zhang, Y.; Yi, Y.; Hu, J. Identification of FeN$_4$ as An Efficient Active Site for Electrochemical N$_2$ Reduction. *ACS Catal.* **2019**, *9*, 7311−7317.

(26) Xu, T.; Ma, D.; Li, T.; Yue, L.; Luo, Y.; Lu, S.; Shi, X.; Asiri, A. M.; Yang, C.; Sun, X. Enhanced Electrocatalytic N$_2$-to-NH$_3$ Fixation by ZrS$_2$ Nanofibers with a Sulfur Vacancy. *Chem. Commun.* **2020**, *56*, 14031−14034.

(27) Chen, G.; Cao, X.; Wu, S.; Zeng, X.; Ding, L.; Zhu, M.; Wang, H. Ammonia Electrosynthesis with High Selectivity under Ambient Conditions via A Li$^+$ Incorporation Strategy. *J. Am. Chem. Soc.* **2017**, *139*, 9771−9774.

(28) Li, C.; Ma, D.; Mou, S.; Luo, Y.; Ma, B.; Lu, S.; Cui, G.; Li, Q.; Liu, Q.; Sun, X. Porous LaFeO$_3$ Nanofiber with Oxygen Vacancies as An Efficient Electrocatalyst for N$_2$ Conversion to NH$_3$ under Ambient Conditions. *J. Energy Chem.* **2020**, *50*, 402−408.

(29) Jin, H.; Li, L.; Liu, X.; Tang, C.; Xu, W.; Chen, S.; Song, L.; Zheng, Y.; Qiao, S.-Z. Nitrogen Vacancies on 2D Layered W$_2$N$_3$: A Stable and Efficient Active Site for Nitrogen Reduction Reaction. *Adv. Mater.* **2019**, *31*, 1902709.

(30) Zhang, X.; Kong, R.; Du, H.; Xia, L.; Qu, F. Highly Efficient Electrochemical Ammonia Synthesis via Nitrogen Reduction Reactions on a VN Nanowire Array under Ambient Conditions. *Chem. Commun.* **2018**, *54*, 5323−5325.

(31) Xia, L.; Li, B.; Zhang, Y.; Zhang, R.; Ji, L.; Chen, H.; Cui, G.; Zheng, H.; Sun, X.; Xie, F.; Liu, Q. Cr$_2$O$_3$ Nanoparticle-Reduced Graphene Oxide Hybrid: A Highly Active Electrocatalyst for N$_2$ Reduction at Ambient Conditions. *Inorg. Chem.* **2019**, *58*, 2257−2260.

(32) Du, H.; Guo, X.; Kong, R.; Qu, F. Cr$_2$O$_3$ Nanofiber: A High-Performance Electrocatalyst Toward Artificial N$_2$ Fixation to NH$_3$ under Ambient Conditions. *Chem. Commun.* **2018**, *54*, 12848−21624.

(33) Yao, D.; Tang, C.; Li, L.; Xia, B.; Vasileff, A.; Jin, H.; Zhang, Y.; Qiao, S. In situ Fragmented Bismuth Nanoparticles for Electrocatalytic Nitrogen Reduction. *Adv. Energy Mater.* **2020**, *10*, 2001289.

(34) Sun, Y.; Deng, Z.; Song, X.; Li, H.; Huang, Z.; Zhao, Q.; Feng, D.; Zhang, W.; Liu, Z.; Ma, T. Bismuth-Based Free-Standing Electrodes for Ambient-Condition Ammonia Production in Neutral Media. *Nano-Micro Lett.* **2020**, *12*, 133.

(35) Qiu, Y.; Zhao, S.; Qin, M.; Diao, J.; Liu, S.; Dai, L.; Zhang, W.; Guo, X. Sandwich-Structured Dual Carbon Modified Bismuth Nanosphere Composites as Long-Cycle and High-Rate Anode Materials for Sodium-Ion Batteries. *Inorg. Chem. Front.* **2020**, *7*, 2006−2016.

(36) Zhang, R.; Ji, L.; Kong, W.; Wang, H.; Zhao, R.; Chen, H.; Li, T.; Li, B.; Luo, Y.; Sun, X. Electrocatalytic N$_2$-to-NH$_3$ Conversion with High Faradaic Efficiency Enabled Using a Bi Nanosheet Array. *Chem. Commun.* **2019**, *55*, 5263−5266.

(37) Li, L.; Tang, C.; Xia, B.; Jin, H.; Zheng, Y.; Qiao, S. Two-Dimensional Mosaic Bismuth Nanosheets for Highly Selective Ambient Electrocatalytic Nitrogen Reduction. *ACS Catal.* **2019**, *9*, 2902−2908.

(38) Montoya, J. H.; Tsai, C.; Vojvodic, A.; Nørskov, J. K. The Challenge of Electrochemical Ammonia Synthesis: A New Perspective on the Role of Nitrogen Scaling Relations. *ChemSusChem* **2015**, *8*, 2180−2186.

(39) Wang, F.; Lv, X.; Zhu, X.; Du, J.; Lu, S.; Alshehri, A. A.; Alzahrani, A. K.; Zheng, B.; Sun, X. Bi Nanodendrites for Efficient Electrocatalytic N$_2$ Fixation to NH$_3$ under Ambient Conditions. *Chem. Commun.* **2020**, *56*, 2107−2110.

(40) Wu, D.; Wang, X.; Fu, X.; Luo, J. Ultrasmall Bi Nanoparticles Confined in Carbon Nanosheets as Highly Active and Durable Catalysts for CO$_2$ Electroreduction. *Appl. Catal., B* **2021**, *284*, 119723.

(41) Zhang, X.; Fu, J.; Liu, Y.; Zhou, X.; Qiao, J. Bismuth Anchored on MWCNTs with Controlled Ultrafine Nanosize Enables High-Efficient Electrochemical Reduction of Carbon Dioxide to Formate Fuel. *ACS Sustainable Chem. Eng.* **2020**, *8*, 4871−4876.

(42) Hao, Y.; Guo, Y.; Chen, L.; Shu, M.; Wang, X.; Bu, T. A.; Gao, W.; Zhang, N.; Su, X.; Feng, X.; Zhou, J. W.; Wang, B.; Hu, C. W.; Yin, A. X.; Si, R.; Zhang, Y. W.; Yan, C. H. Promoting Nitrogen Electroreduction to Ammonia with Bismuth Nanocrystals and Potassium Cations in Water. *Nat. Catal.* **2019**, *2*, 448−456.

(43) Zhang, E.; Wang, T.; Yu, K.; Liu, J.; Chen, W.; Li, A.; Rong, H.; Lin, R.; Ji, S.; Zheng, X.; Wang, Y.; Zheng, L.; Chen, C.; Wang, D.; Zhang, J.; Li, Y. Bismuth Single Atoms Resulting from Transformation of Metal-Organic Frameworks and Their Use as Electrocatalysts for CO$_2$ Reduction. *J. Am. Chem. Soc.* **2019**, *141*, 16569−16573.

(44) Zou, J.; Zhong, W.; Gao, F.; Tu, X.; Chen, S.; Huang, X.; Wang, X.; Lu, L.; Yu, Y. Sensitive Electrochemical Platform for Trace Determination of Pb^{2+} Based on Multilayer Bi-MOFs/Reduced Graphene Oxide Films Modified Electrode. *Microchim. Acta* **2020**, *187*, 603.

(45) Kim, M.-K.; Kim, M.-S.; Park, J.-H.; Kim, J.; Ahn, C.-Y.; Jin, A.; Mun, J.; Sung, Y.-E. Bi-MOF Derived Micro/Meso-Porous Bi@C Nanoplates for High Performance Lithium-Ion Batteries. *Nanoscale* **2020**, *12*, 15214−15221.

(46) Xue, P.; Wang, N.; Fang, Z.; Lu, Z.; Xu, X.; Wang, L.; Du, Y.; Ren, X.; Bai, Z.; Dou, S.; Yu, G. Rayleigh-Instability-Induced Bismuth Nanorod@Nitrogen-Doped Carbon Nanotubes as A Long Cycling and High Rate Anode for Sodium-Ion Batteries. *Nano Lett.* **2019**, *19*, 1998−2004.

(47) Qiu, J.; Li, S.; Su, X.; Wang, Y.; Xu, L.; Yuan, S.; Li, H.; Zhang, S. Bismuth Nano-Spheres Encapsulated in Porous Carbon Network for Robust and Fast Sodium Storage. *Chem. Eng. J.* **2017**, *320*, 300−307.

E

(48) Xiong, W.; Cheng, X.; Wang, T.; Luo, Y.; Feng, J.; Lu, S.; Asiri, A. M.; Li, W.; Jiang, Z.; Sun, X. Co_3(hexahydroxytriphenylene)$_2$: A Conductive Metal-Organic Framework for Ambient Electrocatalytic N_2 Reduction to NH_3. *Nano Res.* **2020**, *13*, 1008−1012.

(49) Xiong, P.; Bai, P.; Li, A.; Li, B.; Cheng, M.; Chen, Y.; Huang, S.; Jiang, Q.; Bu, A. H.; Xu, Y. Bismuth Nanoparticle@Carbon Composite Anodes for Ultralong cycle Life and High-Rate Sodium-Ion Batteries. *Adv. Mater.* **2019**, *31*, 1904771.

(50) Zhu, D.; Zhang, L.; Ruther, R.E.; Hamers, R. J. Photo-Illuminated Diamond as A Solid-State source of Solvated Electrons in Water for Nitrogen Reduction. *Nat. Mater.* **2013**, *12*, 836−841.

(51) Watt, G. W.; Chrisp, J. D. Spectrophotometric Method for the Determination of Hydrazine. *Anal. Chem.* **1952**, *24*, 2006−2008.

(52) Ren, X.; Zhao, J.; Wei, Q.; Ma, Y.; Guo, H.; Liu, Q.; Wang, Y.; Cui, G.; Asiri, A. M.; Li, B.; Tang, B.; Sun, X. High-Performance N_2-to-NH_3 Conversion Electrocatalyzed by Mo_2C Nanorod. *ACS Cent. Sci.* **2019**, *5*, 116−121.

(53) Wei, P.; Xie, H.; Zhu, X.; Zhao, R.; Ji, L.; Tong, X.; Luo, Y.; Cui, G.; Wang, Z.; Sun, X. CoS_2 Nanoparticles-Embedded N-Doped Carbon Nanobox Derived from ZIF-67 for Electrocatalytic N_2-to-NH_3 Fixation under Ambient Conditions. *ACS Sustainable Chem. Eng.* **2020**, *8*, 29−33.